

# Two-Dimensional Simulation of Red Blood Cell Deformation and Lateral Migration in Microvessels

TIMOTHY W. SECOMB,<sup>1</sup> BEATA STYP-REKOWSKA,<sup>2</sup> and AXEL R. PRIES<sup>2,3</sup>

<sup>1</sup>Department of Physiology, University of Arizona, Tucson, AZ 85724-5051, USA; <sup>2</sup>Department of Physiology, Charité – Universitätsmedizin Berlin, Campus Benjamin Franklin, Arnimallee 22, 14195, Berlin, Germany; and <sup>3</sup>Deutsches Herzzentrum Berlin Augustenburger Platz 1, 13353, Berlin, Germany

(Received 5 September 2006; accepted 29 January 2007; published online 23 March 2007)

**Abstract**—A theoretical method is used to simulate the motion and deformation of mammalian red blood cells (RBCs) in microvessels, based on knowledge of the mechanical characteristics of RBCs. Each RBC is represented as a set of interconnected viscoelastic elements in two dimensions. The motion and deformation of the cell and the motion of the surrounding fluid are computed using a finite-element numerical method. Simulations of RBC motion in simple shear flow of a high-viscosity fluid show “tank-treading” motion of the membrane around the cell perimeter, as observed experimentally. With appropriate choice of the parameters representing RBC mechanical properties, the tank-treading frequency and cell elongation agree closely with observations over a range of shear rates. In simulations of RBC motion in capillary-sized channels, initially circular cell shapes rapidly approach shapes typical of those seen experimentally in capillaries, convex in front and concave at the rear. An isolated RBC entering an 8- $\mu\text{m}$  capillary close to the wall is predicted to migrate in the lateral direction as it traverses the capillary, achieving a position near the centerline after traveling a distance of about 60  $\mu\text{m}$ . Cell trajectories agree closely with those observed in microvessels of the rat mesentery.

**Keywords**—Erythrocyte mechanics, Capillary flow, Shear flow, Tank-treading.

## INTRODUCTION

The characteristics of blood flow in the microcirculation are strongly influenced by the presence of red blood cells (RBCs, erythrocytes). Because the dimensions of individual RBCs are comparable to the diameters of the vessels through which they flow, some aspects of microvascular blood flow are not well represented by a continuum model. When blood flows into a diverging microvessel bifurcation, the volume fraction of RBCs (hematocrit) often differs substan-

tially between the two branches<sup>16</sup>. In this “phase separation,” the branch with higher flow typically receives a higher hematocrit. When blood flows along a microvessel, the distribution of hematocrit within the vessel cross-section is non-uniform, with a region of reduced hematocrit near the vessel wall. The presence of this “cell-free layer” causes a substantial reduction of the resistance to flow in capillary-sized tubes relative to the resistance that would be predicted in tubes based on the viscosity of blood as measured in bulk, a phenomenon known as the Fåhræus–Lindqvist effect<sup>10</sup>. The reduction of hematocrit near the wall results from a tendency of RBCs flowing in narrow tubes to migrate away from the wall, across the streamlines of the flow (lateral migration). Thus, the mechanical behavior of RBCs in the microcirculation strongly influences blood flow and oxygen transport to tissue.

Several theoretical approaches have been developed to describe the motion of RBCs in microvessels and its dependence on the mechanical properties of RBCs. Quantitative theoretical models have been developed that successfully predict flow resistance when RBCs flow in single file in narrow capillary-sized tubes.<sup>17,23</sup> In tubes with diameter about 30  $\mu\text{m}$  or more, flow resistance can be predicted using a two-phase continuum model, in which a central core region with uniform viscosity is surrounded by a cell-free layer having an empirically determined width of 1.8  $\mu\text{m}$ .<sup>18,19</sup> However, no quantitative theory is available to predict the width of the cell-free layer from first principles based on the mechanical properties of RBCs. Motions of multiple interacting cells have been simulated in three dimensions using a simplified representation of RBC mechanics<sup>3</sup>. Three-dimensional simulations of the motion of deformable RBCs including realistic membrane properties have so far considered only a single cell in an unbounded domain.<sup>4,15</sup>

Two-dimensional models of deformable RBC motion have previously been developed for single-file

Address correspondence to Timothy W. Secomb, Department of Physiology, University of Arizona, Tucson, AZ 85724-5051, USA. Electronic mail: secomb@u.arizona.edu

flow<sup>22</sup> and for two-file “zipper” flow.<sup>24</sup> Reducing the dimensionality from three to two simplifies the problem, but at the cost of potentially introducing unrealistic features. For example, a model for single-file flow of asymmetric cells<sup>22</sup> predicted of continuous “tank-treading” motion of the cell membrane around the cell interior at a high rate, such that the membrane velocity relative to the cell was up to 50% of the cell velocity. In a subsequent study,<sup>12</sup> three-dimensional tank-treading motion was considered for cells with prescribed three-dimensional shapes. This model took into account the viscous resistance of the cell membrane to shear deformation occurring during tank-treading motion. Predicted tank-treading rates were much lower than those obtained using the two-dimensional model, and corresponded more closely with experimental observations.<sup>9</sup>

The goal of the present study is to develop a two-dimensional model for the motion and deformation of RBCs flowing in microvessels, including fluid mechanical interactions with vessel walls and lateral migration across flow streamlines. Two-dimensional approaches make feasible the simulation of motions of multiple interacting cells.<sup>25,27</sup> In many cases of interest, including the motion of RBCs in shear flow and in capillaries, the RBC shape has a plane of approximate mirror symmetry that is parallel to the flow direction. The present two-dimensional model represents the shape of the cell cross-section in this symmetry plane.

Each cell is represented as an assemblage of a finite number of discrete elements with defined mechanical properties. This approach is taken because it results in a finite set of governing equations for the cell in which the balance of forces acting on each element is exactly satisfied. An alternative approach would be to discretize the continuum equations of membrane equilibrium using a finite-difference or finite-element numerical scheme. Such an approach might not lead to exact force balances. The present approach minimizes numerical errors that could affect predictions regarding lateral migration of cells. Although numerical errors resulting from the discretization of the fluid flow field are not eliminated, such errors are controlled by the finite-element software (see below).

The properties of the model are chosen to represent the mechanical behavior of RBCs as closely as possible subject to the constraints of two-dimensionality. In particular, internal viscous elements are introduced to represent the effects of viscous resistance of the membrane to shear deformation that it experiences in three-dimensional deformations and the viscosity of the cell interior. Model parameters are estimated by matching predictions with observations of continuous “tank-treading” motion of the cell membrane around the cell that is observed when RBCs are placed in dilute

suspension in a high-viscosity medium and subjected to simple shear flow.<sup>8</sup> The model is then used to predict the deformation and lateral migration of RBCs in microvessels. Predictions are compared with corresponding experimental observations made using glass tubes and microvessels of the rat mesentery.

## METHODS

### Formulation of the Mechanical Model

The two-dimensional representation of RBC mechanics is shown in Fig. 1. The outline represents the cross-sectional shape of a three-dimensional cell in a plane through the center of the cell (the “model cell plane”). The cell membrane lying in this plane is represented as a chain of straight elements, hinged at the nodal points. Each element consists of an elastic

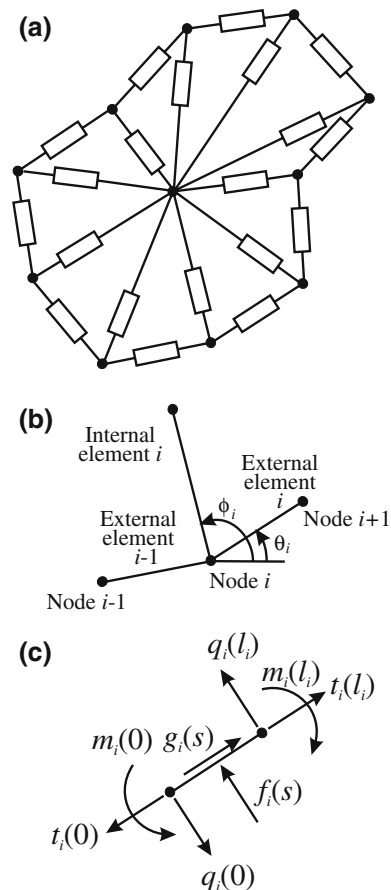


**FIGURE 1.** (a) Schematic view of two-dimensional model for RBC. Rectangles denote viscoelastic elements of variable length, connected at nodes. (b) Numbering scheme for nodes and elements. The angles of external element  $i$  and internal element  $i$  to the reference direction are denoted by  $\theta_i$  and  $\phi_i$ . (c) Forces and loads acting on segment  $i$ . The longitudinal force  $t_i(s)$ , the transverse force  $q_i(s)$  and the bending moment  $m_i(s)$  vary along the segment, and the forces indicated are the resultants acting on the two ends.

component in parallel with a viscous component, thus representing the viscoelastic response of the membrane to deformation (elongation or shortening) in the model cell plane.<sup>11</sup> The resistance of the membrane to bending is represented by making the nodes (hinge points) between the membrane elements elastic. A bending moment is introduced at each node that is proportional to the angle between successive segments.

The mechanical model includes internal viscous elements that connect each nodal point to a single central point within the model cell (Fig. 1). These elements are included to represent the viscous resistance of a three-dimensional cell to tank-treading motions, resulting both from the shear viscosity of the cell membrane and the viscosity of the fluid in the cell interior. In such flows, the cell typically assumes an elongated, approximately ellipsoidal shape, aligned almost parallel to the flow direction. A band of membrane around the cell (i.e., out of the model cell plane) is alternately lengthened and shortened by the tank-treading motion (Fig. 2). This continuous deformation of membrane results in viscous energy dissipation in the membrane<sup>6</sup> and resistance to tank-treading motion. The fluid interior of the cell is viscous and resists tank-treading motion. Fischer<sup>6</sup>

estimated that the viscous dissipation in the interior is less than or equal to the viscous energy dissipation in the cell membrane for tank-treading and other motions. These two effects, the viscous resistance of the membrane to deformation out of the model cell plane and the internal viscosity of the cell, are lumped together in the two-dimensional model and simulated by the internal viscous elements, avoiding the computation of the internal flow field. The fluid in the cell is assumed to exert a constant pressure on the membrane.

### Governing Equations of the Cell

The nodes and segments are numbered as shown in Fig. 1b, where  $1 \leq i \leq n$  and  $n$  is the number of external nodes and elements. The external elements are subjected to loadings resulting from the fluid flow around the model cell. As a result, the longitudinal (tension) force  $t_i(s)$ , the transverse (shear) force  $q_i(s)$  and the bending moment  $m_i(s)$  acting in external element  $i$  are functions of distance  $s$  along the element from node  $i$  to node  $i + 1$ , where  $0 \leq s \leq l_i$ , and  $l_i$  is the length of the element. As usual in membrane mechanics, these quantities are expressed as force per unit length. The equations of mechanical equilibrium for the element are

$$dt_i/ds = -g_i \quad (1)$$

$$dq_i/ds = -f_i \quad (2)$$

$$dm_i/ds = q_i \quad (3)$$

where  $f_i(s)$  and  $g_i(s)$  are the normal and tangential components of the fluid loading, as indicated in Fig. 1c. It is useful to define the mean tension  $\bar{t}_i$  and the mean shear  $\bar{q}_i$  in each element as follows:

$$\bar{t}_i = \frac{1}{l_i} \int_0^{l_i} t_i(s) ds \quad \text{and} \quad \bar{q}_i = \frac{1}{l_i} \int_0^{l_i} q_i(s) ds \quad (4)$$

To represent the viscoelastic behavior of the external segments, the mean tension in external element  $i$  is given by

$$\bar{t}_i = k_t(l_i/l_0 - 1) + \mu_m \frac{1}{l_i} \frac{dl_i}{dt} \quad (5)$$

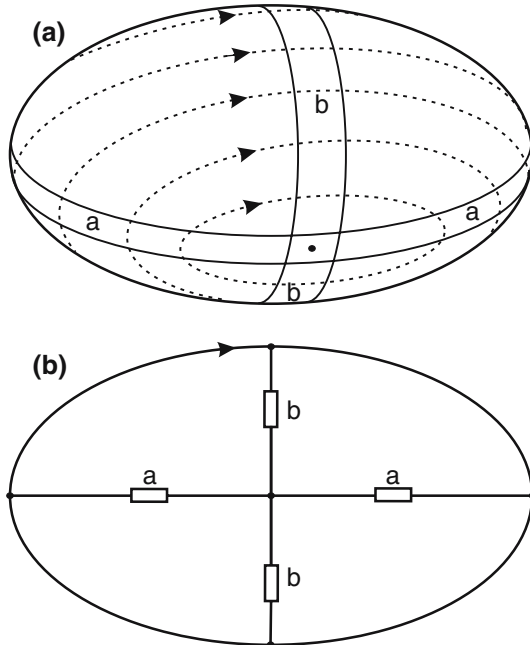


**FIGURE 2.** Relationship between internal viscous elements and membrane deformation in tank-treading. (a) Dashed lines and arrows indicate tank-treading motion of membrane on an ellipsoid, representing a three-dimensional RBC. Circumferential band of membrane is alternately lengthened [a] and shortened [b] as a result of this motion. (b) Corresponding two-dimensional representation as used in present model. Internal viscous elements are alternately lengthened [a] and shortened [b] during tank-treading motion (arrow).

where  $l_0$  is the reference length of the element,  $k_t$  is the elastic modulus and  $\mu_m$  is the viscosity. The bending moments acting on element  $i$  at nodes  $i$  and  $i + 1$  are given by

$$m_i(0) = -k_b \alpha_i / l_0 \text{ and } m_i(l_i) = -k_b \alpha_{i+1} / l_0$$

where  $k_b$  is the bending modulus and  $\alpha_i = \theta_i - \theta_{i-1}$  is the angle between elements  $i-1$  and  $i$  (Fig. 1b). The factor  $l_0$  is included to convert  $\alpha_i$  to a curvature. Integrating Eq. (3) gives

$$\bar{q}_i = k_b (\alpha_i - \alpha_{i+1}) / (l_0 l_i). \quad (6)$$

By applying integration by parts to Eq. (4) and using Eqs. (1) and (2), the tension and shear forces at each end of the element can be expressed in terms of the mean values and the loadings:

$$\begin{aligned} t_i(0) &= \bar{t}_i + \frac{1}{l_i} \int_0^{l_i} g_i(s)(l_i - s) ds, \\ t_i(l_i) &= \bar{t}_i - \frac{1}{l_i} \int_0^{l_i} g_i(s) s ds, \end{aligned} \quad (7)$$

$$\begin{aligned} q_i(0) &= \bar{q}_i + \frac{1}{l_i} \int_0^{l_i} f_i(s)(l_i - s) ds, \\ q_i(l_i) &= \bar{q}_i - \frac{1}{l_i} \int_0^{l_i} f_i(s) s ds. \end{aligned} \quad (8)$$

The internal elements are assumed to have viscous resistance to changes in length, giving

$$T_i = \mu'_m \frac{1}{L_i} \frac{dL_i}{dt} \quad (9)$$

where  $L_i$  is the length of internal element  $i$  and  $\mu'_m$  is its viscosity. The conditions for overall equilibrium of forces acting at node  $i$  are

$$\begin{aligned} t_i(0) \cos \theta_i - t_{i-1}(l_{i-1}) \cos \theta_{i-1} - q_i(0) \sin \theta_i \\ + q_{i-1}(l_{i-1}) \sin \theta_{i-1} + T_i \cos \varphi_i = 0, \end{aligned} \quad (10)$$

$$\begin{aligned} t_i(0) \sin \theta_i - t_{i-1}(l_{i-1}) \sin \theta_{i-1} + q_i(0) \cos \theta_i \\ - q_{i-1}(l_{i-1}) \cos \theta_{i-1} + T_i \sin \varphi_i = 0. \end{aligned} \quad (11)$$

Equilibrium of forces at the central node implies that

$$\sum_{i=1}^n T_i \cos \varphi_i = \sum_{i=1}^n T_i \sin \varphi_i = 0. \quad (12)$$

For any given configuration of the cell (i.e., for known positions of the nodes), Eqs. (5–9) can be used to express the equilibrium equations (10–12) as a linear system involving the fluid loads  $f_i(s)$  and  $g_i(s)$  on each external segment and the velocities of the nodes. This system is coupled to the equations of fluid motion, as described below.

The interior of a three-dimensional RBC is effectively incompressible, so that it deforms at constant volume, and the membrane deforms at nearly constant surface area. In the two-dimensional model, these constraints cannot be explicitly imposed because the cell shape is not defined outside the model cell plane. The analogous properties of the two-dimensional model, the perimeter and area in the model cell plane, are not constants. However, they are restricted to relatively narrow ranges reflecting the possible shapes of a three-dimensional cell with fixed surface area and volume. In the model, variations of perimeter are resisted by the elastic control of individual segment lengths, Eq. (5), while variations of cell area  $A$  are resisted by assigning a pressure to the interior of the cell:

$$p_{\text{int}} = k_p (1 - A/A_{\text{ref}}) \quad (13)$$

where  $A_{\text{ref}}$  and  $k_p$  are constants.

#### *Equations of Fluid Motion and Numerical Methods*

The suspending medium is assumed to be a viscous incompressible fluid, and the Reynolds number is assumed to be extremely small, so that inertial effects can be neglected and the governing equations are those of Stokes flow. The pressure and velocity fields are expressed in two-dimensional coordinates  $(x, y)$  as  $p(x, y)$  and  $\mathbf{u}(x, y)$  where  $\mathbf{u} = (u, v)$ . The components of stress in the fluid are then

$$\begin{aligned} \sigma_{xx} &= 2\mu \partial u / \partial x - p, \quad \sigma_{xy} = \mu (\partial v / \partial x + \partial u / \partial y) \text{ and} \\ \sigma_{yy} &= 2\mu \partial v / \partial y - p. \end{aligned} \quad (14)$$

Conservation of momentum implies that  $\partial \sigma_{xx} / \partial x + \partial \sigma_{xy} / \partial y = 0$  and  $\partial \sigma_{xy} / \partial x + \partial \sigma_{yy} / \partial y = 0$ . (15)

The divergence of the velocity field is defined by

$$e = \partial u / \partial x + \partial v / \partial y \quad (16)$$

where  $e = 0$  in an incompressible flow. The fluid loadings at a point on external element  $i$  are related to the local components of fluid stress by the equations:

$$f_i = -p_{\text{int}} - \sigma_{xx} \sin^2 \theta_i + 2\sigma_{xy} \sin \theta_i \cos \theta_i - \sigma_{yy} \cos^2 \theta_i, \quad (17)$$

$$g_i = (\sigma_{xx} - \sigma_{yy}) \sin \theta_i \cos \theta_i - \sigma_{xy} (\cos^2 \theta_i - \sin^2 \theta_i). \quad (18)$$

The fluid velocity adjacent to the cell must match the local cell velocity according to the no-slip condition. The velocity at each point on a given external element is obtained by linear interpolation between the nodal velocities at the ends of the segment. Conditions on the velocity and pressure at the external boundaries of the fluid domain are chosen according to the flow to be considered, such as a linear shear flow or a pressure-driven channel flow.

The resulting system of coupled equations for the motion of the cell and the surrounding fluid was solved using a finite element package (FlexPDE version 3.11, PDE Solutions Inc., Antioch, CA). Quadratic elements were used. Because of the structure of FlexPDE, the incompressibility condition  $e = 0$  cannot be specified as one of the governing equations. As suggested in the documentation accompanying FlexPDE, the condition  $e = 0$  can be satisfied approximately by setting

$$\nabla^2 p = Ke \quad (19)$$

where  $K$  is a large constant. At any point where  $e > 0$ , this condition would induce a local reduction in  $p$ , tending to drive fluid towards that point, and conversely if  $e < 0$ . Therefore,  $e$  must remain close to zero. Values of  $e$  were monitored to ensure that they remained small. Root mean square values were less than 2% of typical velocity gradients. The components ( $u_i, v_i$ ) of velocity at node  $i$  and at the central node were introduced into the finite element formulation as scalar variables. The corresponding Eqs. (10–12) were solved simultaneously with the equations resulting from the finite element formulation of Eqs. (15) and (19).

Generally,  $n = 20$  nodes were used to represent the RBC shape. The number of fluid elements was typically in the range 100–400. A sample mesh is shown in Fig. 3. The mesh is automatically generated by the finite element package. In cases where a cell closely

approaches the domain boundary, the mesh generator controls the aspect ratio of the elements, so that a large number of small elements are used. This allows resolution of steep pressure and velocity gradients, which may occur in such regions. The finite-element software automatically refines the mesh until solution errors are within a specified tolerance.

At each time step, the nodal velocities and the fluid velocity and pressure fields were computed for a given cell shape. The cell shape was then updated according to the computed nodal velocities and the specified time step using an explicit (Euler) scheme. This procedure was repeated to generate a sequence of cell shapes, which could be represented using still or moving images. Because an explicit scheme is used, the time step is limited by the requirement for numerical stability. If the time step is too large, a typical instability involves oscillations of nodal positions at successive time steps. In most cases, a time step of 1 ms was used. Smaller time steps were used for calculations of cell motions in shear flow at high shear rates and viscosities. One source of numerical instability is the condition that deformation occurs at approximately constant area. Larger values of the constant  $k_p$  in Eq. (13) would require smaller time steps. Computational time

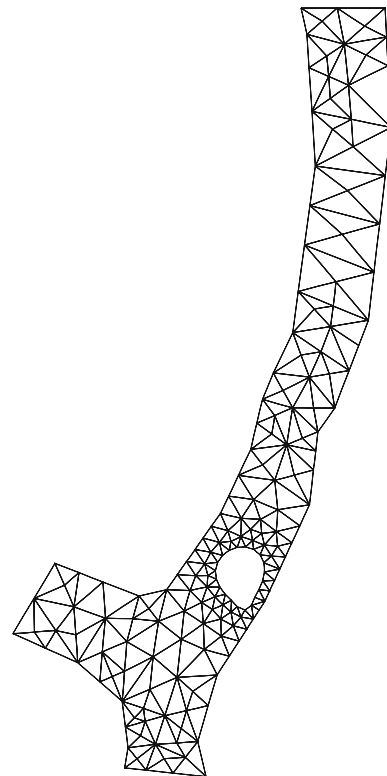


FIGURE 3. Example of finite-element mesh used, with 277 quadratic elements.

depends on the complexity of the mesh. For the case shown in Fig. 3, each time step required approximately 100 s on a personal computer with a 2 GHz processor.

An essential aspect of the deformability of RBCs is that their sphericity index (s.i.) is less than 1. The s.i. is a dimensionless combination of volume and surface area, such that s.i. = 1 for spheres and s.i. < 1 for all other shapes. For human RBCs, the s.i. is normally in the range 0.72–0.86.<sup>1</sup> For the model two-dimensional cells, an analogous ‘circularity index’ (c.i.) of a two-dimensional cell shape may be defined as  $2(\pi A_{\text{ref}})^{1/2}/(nl_0)$ , where  $nl_0$  is the reference perimeter. For the parameter values used here (see below), c.i. = 0.86. The initial shape was assumed to be circular with area  $A_{\text{ref}}$ . In this configuration, each external element is compressed to a length less than its reference length  $l_0$ . As the motion proceeds, the segments elongate and the cell perimeter increases, allowing non-circular shapes with the same area. The circular initial shape was chosen so that the subsequent motion does not depend on the initial orientation of the cell and reflects only its initial position and the nature of the flow field in which it is suspended.

#### *Scaling and Parameter Values*

Scaled values of all variables were used both for numerical convenience and because the scaling itself provides insight into the relative magnitudes of the quantities involved. All distances are expressed in  $\mu\text{m}$  and all times in ms. With this scaling, velocities are in mm/s, which is a typical scale of blood flow in microvessels. Forces are expressed in units of  $10^{-7}$  dyn. The corresponding unit of viscosity is then 1 cP ( $10^{-2}$  dyn s/cm<sup>2</sup>), close to the viscosity of normal blood plasma. The corresponding unit of pressure and stress is 10 dyn/cm<sup>2</sup>. The shear elastic modulus, bulk (area) modulus and bending resistance of the membrane are estimated to be  $1.8 \times 10^{-12}$  dyn cm, 0.006 dyn/cm, and 500 dyn/cm.<sup>5,11</sup> The corresponding scaled values are 0.18 for bending modulus, 6 for shear modulus, and  $5 \times 10^5$  for bulk modulus. From these values, it is evident that elastic bending resistance is generally a small effect, shear resistance is significant and resistance to area change is very high. The shear viscosity of the membrane is estimated to be 0.001 dyn s/cm,<sup>11</sup> corresponding to a scaled value of 1000. Therefore, the cell has a large viscous resistance to deformation on the millisecond timescale. The disparate values of these scaled parameters are indicative of the difficulties encountered in simulating the motion of deformable RBCs. For instance, the small scaled bending resistance allows for the development of regions of high membrane curvature,<sup>23</sup> while the large scaled viscosity implies that rapid deformations of cells suspended in low-viscosity media such as plasma are only generated

when cells interact closely with each other or the flow boundaries, such that large forces are generated.<sup>21</sup> Some calculations at large levels of shear stress were done with a scaled bending modulus of 0.9, to inhibit numerical instabilities resulting from low bending resistance. In such instabilities, the angle between segments at one or more nodes increases beyond 180° over several time steps. The constants used to limit changes in cell area (Eq. 13) and to enforce fluid incompressibility (Eq. 19), were typically set to  $k_p = 50$ , i.e., 500 dyn/cm<sup>2</sup>, and  $K = 100$ , i.e., 1 dyn s/cm<sup>2</sup>.

In the model, the membrane shear and bending elastic moduli are represented by the parameters  $k_t$  and  $k_b$ , and the shear viscosity is represented by the parameters  $\mu_m$  and  $\mu'_m$ . The values of these parameters should be similar in magnitude to the scaled values given above, although an exact correspondence cannot be made because the two-dimensional model does not explicitly describe membrane shear deformations. For this reason, the approach is not well suited for deducing actual mechanical properties of RBCs from experimental observations. Values for the membrane parameters  $k_t$ ,  $\mu_m$  and  $\mu'_m$  and the geometric parameters  $l_0$  and  $A_{\text{ref}}$  used in the model were obtained by adjusting them to provide a good fit to experimentally observed behavior of RBCs tank-treading in simple shear flow of high-viscosity media, including variation of cell length and tank-treading frequency with shear rate. Further simulations were then performed using channel geometries representative of red cell motion in capillaries, including effects of asymmetric cell position.

#### *Observations of RBC Motion in Rat Mesenteric Microvessels*

Animal experiments were carried out in accordance with University and State regulations and after obtaining approval by the authorities for animal welfare. Two male Sprague–Dawley rats (300 g bw), were anesthetized (urethane, 100 mg/kg i.p. and ketavet, 100 mg/kg i.m.). Catheters were inserted into the carotid artery to allow blood sampling for blood gas analysis and monitoring of mean arterial pressure and into the jugular vein for continuous infusion of buffered physiological saline (24 ml/kg per hour). The mesentery was removed from the abdominal cavity of the rat and was kept in a bath filled with buffered physiological saline at a temperature 37°C. An intestinal segment with the attached mesenteric vascular bed was placed on a cylindrical platform with a circular glass window allowing Koehler type transillumination. Illumination was achieved with a video triggered xenon flash strobe (Strobex, Model 11360 Chadwick-Helmuth, El Monte, CA USA) such that

each video field received one flash (time delay between flashes 20 ms). In some recordings, two flashes 10 ms apart were generated during each video frame. Microscopic images were generated with a 50 $\times$ , NA1.0 salt water immersion objective (Leica, Wetzlar, Germany) and stored on a digital video tape recorder (Type DSR 45P DVCAM, Sony).

In each mesentery, a diverging microvascular bifurcation was selected in which one branch received relatively low flow, and therefore low hematocrit,<sup>16</sup> such that isolated RBCs occasionally entered the branch vessel, preceded by a plasma gap. Video sequences recording the passage of such RBCs along the visible portion of the branch were analyzed using an image analysis system consisting of a frame grabber (Corona II, Matrox, Dorval, Canada) and a proprietary software allowing the interactive tracing and digitizing of outlines of the selected cells on successive video fields. The wall outline was also digitized and used as the domain boundary for corresponding numerical simulations.

#### Observations of Human RBC Motion In Vitro

Glass tubes with inside diameter 7  $\mu\text{m}$  were drawn from larger bore tubes and mounted on the stage of a microscope with an oil-immersion objective. Blood from healthy volunteers was anticoagulated with heparin, centrifuged, and resuspended in isotonic Krebs-Ringer solution at hematocrit 0.2. The suspension was passed through the tube with a fixed pressure drop such that red cells moved with velocity  $\sim 1$  mm/s.

## RESULTS

Figure 4 shows the predicted behavior of a RBC suspended in a high viscosity medium (13 cP) and subjected to a simple shear flow. Starting from a circular initial shape, the cell quickly approaches a stable elongated shape aligned at a constant small angle to the flow direction. Examples of the eventual shapes are shown in Fig. 4a. Each node and segment in the cell progresses steadily around the cell, in a tank-treading motion whose frequency is defined by the successive returns of a node in the membrane to a given location relative to the cell shape. With increasing shear rates, the equilibrium cell shapes become more elongated, as observed experimentally.<sup>8</sup> Although the cell shapes have rotational symmetry, they do not show mirror symmetry, but have distinctive counter-clockwise twists at the extremities. It is not known whether this feature is present in reality, since available images are obtained from the perpendicular direction in which such features would not be visible.<sup>8</sup> The computed shapes share some

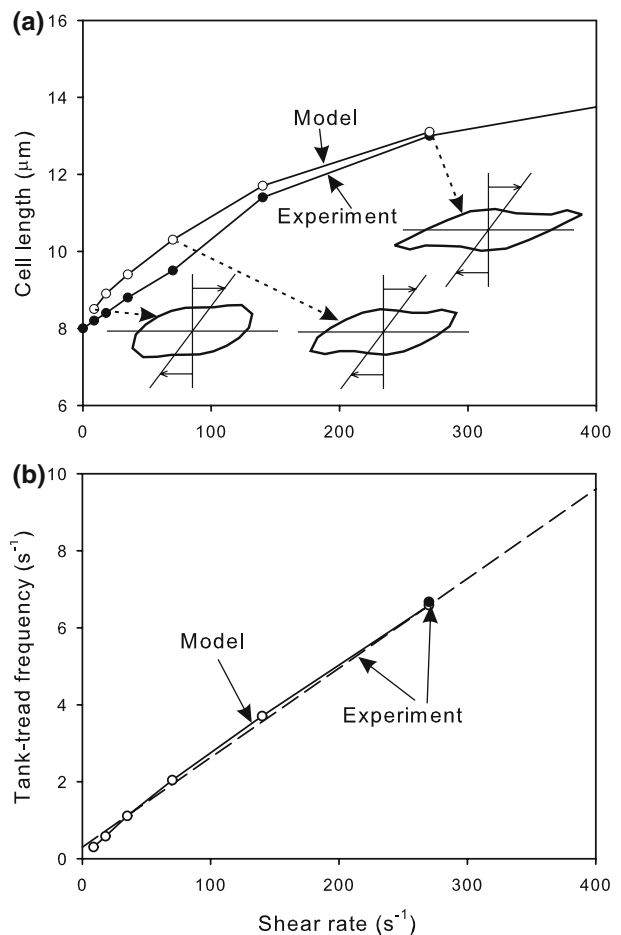


**FIGURE 4.** Predicted and observed behavior of a tank-treading cell, suspended in a linear simple shear flow. Suspending medium viscosity is 13 cP. (a) Overall length in the flow direction. Open symbols: model predictions. Solid symbols: Measured values based on photographs,<sup>19</sup> assuming a cell diameter of 8  $\mu\text{m}$  in the unstressed state. Insets show predicted equilibrium cell shapes, at shear rates of 8.7, 70 and 270  $\text{s}^{-1}$ . Diagonal lines and arrows within insets indicate orientation of imposed simple shear flow. (b) Tank-treading frequency. Open symbols: model predictions. Solid symbol: measured value based on photographs.<sup>19</sup> Dashed line: regression line of experimental data from multiple experiments with viscosities ranging from 11 to 59 cP.<sup>7</sup>

features with those observed when surfactant-laden drops are placed in simple shear flow.<sup>2</sup>

The overall length of the cell measured in the flow direction and the frequency of the tank-treading motion were computed for a range of imposed shear rates from 8.7 to 270  $\text{s}^{-1}$ . The unknown parameters were then adjusted so as to achieve close agreement with corresponding experimental data<sup>7,19</sup> as shown in Fig. 4. The resulting scaled parameter values, which were used in the subsequent computations, were:  $k_t = 12$  (i.e., 0.012 dyn/cm), representing membrane shear elasticity;  $\mu_m = 100$  (i.e., 0.0001 dyn s/cm), representing membrane viscous resistance to in-plane

deformation;  $\mu'_m = 200$  (i.e., 0.0002 dyn s/cm), representing effects of internal viscosity and of membrane viscous resistance to out-of plane deformation; reference segment length  $l_0 = 0.97 \mu\text{m}$ ; and reference cell area  $A_{\text{ref}} = 22.2 \mu\text{m}^2$ . This set of values was not unique, and other similar sets of values produced almost identical results. However, large changes in parameter values produced results that were not compatible with the observations. For example, if the viscosity of the internal elements was not included (by setting  $\mu'_m = 0$ ), the tank-treading frequency was much higher than observed: at a shear rate  $70 \text{ s}^{-1}$ , the predicted frequency was then  $4.7 \text{ s}^{-1}$  versus the observed frequency,  $2 \text{ s}^{-1}$ . The values of  $\mu_m$  and  $\mu'_m$  (0.0001 and 0.0002 dyn s/cm) obtained by this procedure were smaller than expected based on a membrane shear viscosity of 0.001 dyn s/cm. However, the values obtained are consistent with previous estimates of membrane shear viscosity based on observations of RBC tank-treading frequency.<sup>12,26</sup>

If the viscosity of the external medium is below a critical level, the steady tank-treading motion of an isolated RBC in shear flow is replaced by a tumbling motion.<sup>13</sup> The present model is capable of predicting such a motion. Simulations were carried out with external viscosity 1 cP and shear rate  $350 \text{ s}^{-1}$ . Within the first several milliseconds, the imposed shear flow broke the initial circular symmetry of the cell shape, causing it to become elliptical, and the cell then tumbled as expected.

The predicted motions and deformations of cells flowing in an  $8\text{-}\mu\text{m}$  channel, representative of a microvessel, are summarized in Fig. 5. Cell velocity in each case is about  $1.25 \text{ mm/s}$ . The parameter  $y_0$  gives the initial distance of cell's center from the centerline of the channel. As cells progress along the channel, they rapidly approach shapes similar to those observed in capillaries, convex in front and concave at the rear (Fig. 5c). This change in shape is accompanied by an increase in cell length from the initial circular shape and a slight decrease in width (Fig. 5b). Cells whose initial positions are off the center-line develop asymmetric shapes, more elongated on the side close to the wall. They also show a tendency to migrate towards the center-line, particularly in the first 50 ms of the motion, during which they travel about  $60 \mu\text{m}$  (Fig. 5a). Experimentally observed RBC shapes in a  $7\text{-}\mu\text{m}$  glass tube are shown for comparison (Fig. 5d). Predicted cell shapes closely resemble the observed shapes.

Further simulations were performed to predict the motion of RBCs in specific microvascular geometries observed in the rat mesentery. Figure 6a and b shows the regions selected for observation, and Fig. 6c and d shows the digitized outlines of the vessels and of the isolated RBCs as observed in successive video frames.

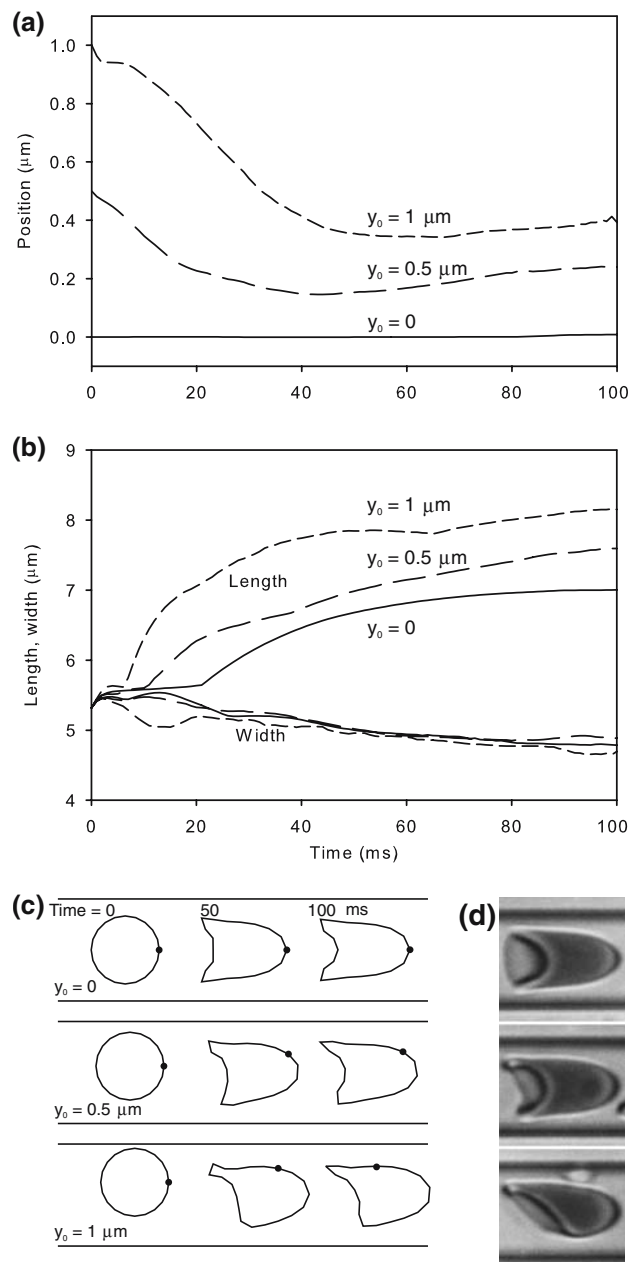


**FIGURE 5.** Predicted motion and deformation of cells flowing in an  $8\text{-}\mu\text{m}$  channel. Flow rate is adjusted so that cell velocity is approximately  $1.25 \text{ mm/s}$ . Results are presented for cells with initial positions  $y_0 = 0, 0.5, 1 \mu\text{m}$  (solid lines, long dashes, short dashes). (a) Position of cell's center of mass, relative to channel center-line, as function of time. (b) Cell length and width as functions of time. (c) Predicted cell shapes initially and after 50 and 100 ms. Dot on cell outline represents a node fixed in the cell. (d) Observed human RBC shapes in a single glass capillary with diameter  $7 \mu\text{m}$ . Three cells are shown with varying orientations and degrees of asymmetry. Direction of flow is left to right in (c) and (d).

In the simulations, the initial positions of the cell were chosen so that the cells entered the branch vessel at approximately the same position as the observed isolated RBCs. The flow rates were adjusted so that the



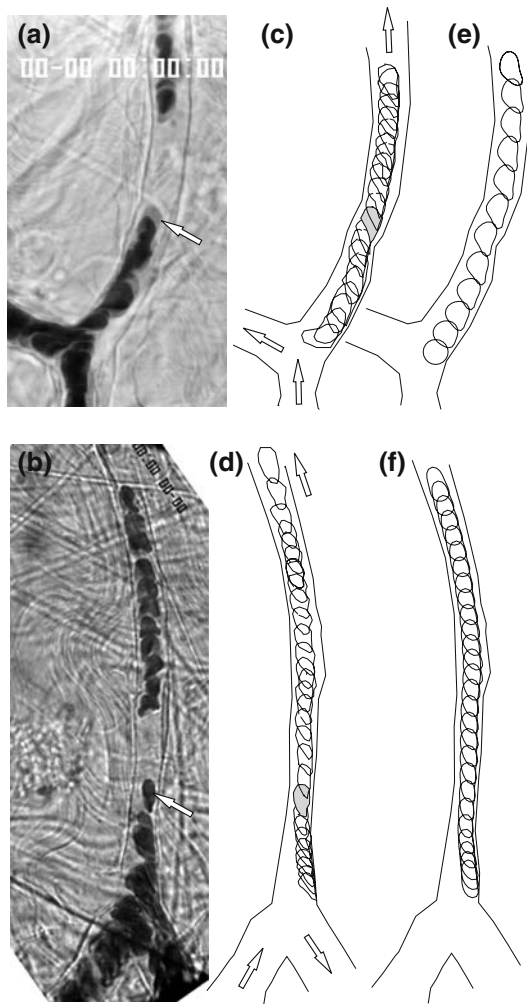


**FIGURE 6.** Observations and simulations of RBC motion in mesenteric microvessels. (a, b) Mesenteric microvessels selected for observation. Arrows indicate isolated RBCs whose motion was tracked. In (a), double-flash illumination was used; regions occupied by a cell at one flash only appear gray. (c, d) Superimposed digitized outlines of vessel wall and of selected isolated cells, observed in successive video frames at intervals of 10 and 20 ms, respectively. Arrows show flow directions. (e, f) Simulated RBC motion. Predicted cell shapes at intervals of 20 ms are shown superimposed on the measured wall outline, which was used as the flow domain in the computations.

predicted RBC velocities were close to the observed values. Corresponding model results are shown in Fig. 6e and f. Close agreement between observed and simulated motion is seen.

In the case of the region shown in Fig. 6a, several isolated RBCs entered the downstream branch with distinctly different initial positions during the observation period. Sequences of frames showing trajectories of six individual cells were recorded and the cell outlines were digitized. For each cell, the trajectory of the center of mass was computed from the digitized cell

outlines. For one frame in each sequence, the outline of the wall was also digitized and combined with the computed trajectory. To correct for tissue movement between sequences, the resulting images were graphically aligned so that the corresponding wall outlines coincided as closely as possible. The resulting combined image is shown in Fig. 7a. RBC trajectories that are initially about  $4\ \mu\text{m}$  apart converge within about  $1\ \mu\text{m}$  in a distance of less than  $30\ \mu\text{m}$ . Corresponding simulated cell trajectories are shown in Fig. 7b, for five different initial cell positions. The computed trajectories are superimposed on the observed trajectories in Fig. 7c, and close correspondence between experimental and simulated motions is again evident.

## DISCUSSION

Effects of the particulate nature of blood on its flow in microvessels, including the formation of a cell-free layer, were recognized as early as the 18th century.<sup>10</sup> However, theoretical analysis of these effects is difficult, because they involve the interaction of multiple, highly deformable particles with the non-uniform flow geometry presented by the microcirculation. The approach presented here addresses this problem. In this approach, each RBC is represented by a two-dimensional assembly of viscoelastic mechanical elements. Use of a two-dimensional model greatly reduces the computational difficulty of the problem. The inclusion of internal viscous elements (Fig. 1a) provides an approximate representation of three-dimensional aspects of cell deformation, particularly stretching of the membrane in the out-of-plane direction. This approach is supported by the close quantitative agreement between observed and simulated tank-treading behavior of RBCs (Fig. 3).

When applied to the simulation of flow in microvessels, the model successfully reproduces several significant experimentally observed phenomena. Actual RBC shapes seen in a  $7\text{-}\mu\text{m}$  glass tube are inherently three-dimensional, and may be described as “slipper-shaped” (Fig. 5d). Even so, predicted RBC shapes surprisingly well with the observed shapes (Fig. 5), given the limitations of a two-dimensional model. In all cases considered here, the cell shape has approximate mirror symmetry about a plane parallel to the flow direction. The model would be expected to be less effective where symmetry is not present, as for example when an arbitrarily oriented slipper-shaped cell approaches a flow divider in a bifurcation, or an arbitrarily oriented disk-shaped cell is suspended in a shear flow at very low shear rate. Furthermore, the present model is not suitable for estimating flow resistance in capillary-size tubes containing RBCs,

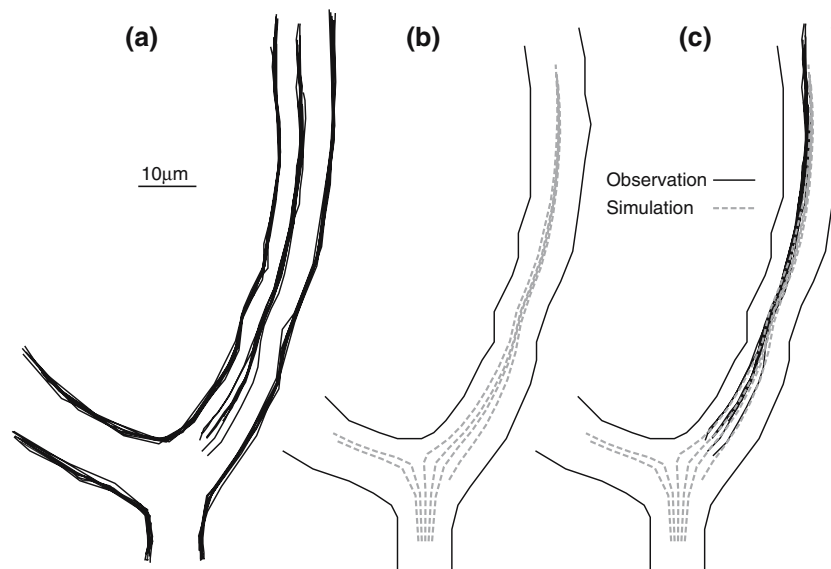


**FIGURE 7.** Observation and simulation of RBC trajectories in mesenteric microvessels. (a) Observed trajectories of six RBCs downstream of the bifurcation shown in Fig. 5a. (b) Computed RBC trajectories for five different initial cell positions. (c) Superimposed image of observed and computed trajectories.

because effects of particles of a given size on flow resistance are different in tube and channel geometries.

The experimental studies in rat mesentery show that the trajectories of isolated RBCs flowing along a microvessel from different starting positions tend to converge to a single trajectory. Within  $30\ \mu\text{m}$ , the spread in the trajectories is reduced from  $4\ \mu\text{m}$  to about  $1\ \mu\text{m}$ . The simulations reproduce this behavior to a good approximation, and provide some insight into the mechanisms of lateral migration. Well known symmetry arguments can be used to obtain conditions for lateral migration in Stokes flow. For example, an isolated rigid object with fore-aft symmetry (with respect to a plane perpendicular to the flow direction) cannot show lateral migration. In the simulations, the initially circular cell shape changes quickly to an asymmetric shape (Fig. 5). The pressure gradient generates a fore-aft asymmetry, while off-axis cells develop lateral asymmetry. Such asymmetries in shape can result in lateral migration.<sup>14,20</sup> For rigid closely fitting particles flowing in tubes, damped oscillatory motions have been predicted for certain particle shapes.<sup>20</sup> This may explain the fact that migration to the centerline reverses after finite time (Fig. 5a). However, further work is needed to gain a more complete understanding of this phenomenon with respect, for example, to the relative roles of shape asymmetry and continuing deformation in migration. Where multiple RBCs are present, cell-cell interactions are likely to play a major role in determining the extent of lateral migration and the width of the cell-free layer. The method presented here can be used to simulate such cases, which will be the subject of future work.

## ACKNOWLEDGMENTS

Supported by NIH Grant HL034555.

## REFERENCES

- <sup>1</sup>Burton, A. C. *Physiology and Biophysics of the Circulation*. Year Book Medical Publishers, Chicago, 1972.
- <sup>2</sup>Debruijn, R. A. Tipstreaming of drops in simple shear flows. *Chem. Eng. Sci.* 48:277–284, 1993.
- <sup>3</sup>Dzwiniel, W., K. Boryczko, and D. A. Yuen. A discrete-particle model of blood dynamics in capillary vessels. *J. Colloid Interface Sci.* 258:163–173, 2003.
- <sup>4</sup>Eggleton, C. D., and A. S. Popel. Large deformation of red blood cell ghosts in a simple shear flow. *Phys. Fluids* 10:1834–1845, 1998.
- <sup>5</sup>Evans, E. A. Bending elastic modulus of red blood cell membrane derived from buckling instability in micropipet aspiration tests. *Biophys. J.* 43:27–30, 1983.
- <sup>6</sup>Fischer, T. M. On the energy dissipation in a tank-treading human red blood cell. *Biophys. J.* 32:863–868, 1980.
- <sup>7</sup>Fischer, T. M., M. Stöhr, and H. Schmid-Schönbein. Red blood cell (rbc) microrheology: Comparison of the behavior of single rbc and liquid droplets in shear flow. *AIChE Symp. Ser. No. 182*, 74:38–45, 1978.
- <sup>8</sup>Fischer, T. M., M. Stöhr-Lissen, and H. Schmid-Schönbein. The red cell as a fluid droplet: Tank tread-like motion of the human erythrocyte membrane in shear flow. *Science* 202:894–896, 1978.
- <sup>9</sup>Gahtgens, P., and H. Schmid-Schönbein. Mechanisms of dynamic flow adaptation of mammalian erythrocytes. *Naturwissenschaften* 69:294–296, 1982.
- <sup>10</sup>Goldsmith, H. L., G. R. Cokelet, and P. Gahtgens. Robin Fahraeus: Evolution of his concepts in cardiovascular physiology. *Am. J. Physiol.* 257:H1005–H1015, 1989.
- <sup>11</sup>Hochmuth, R. M., and R. E. Waugh. Erythrocyte membrane elasticity and viscosity. *Annu. Rev. Physiol.* 49:209–219, 1987.

- <sup>12</sup>Hsu, R., and T. W. Secomb. Motion of nonaxisymmetric red blood cells in cylindrical capillaries. *J. Biomech. Eng.* 111:147–151, 1989.
- <sup>13</sup>Keller, S. R., and R. Skalak. Motion of a tank-treading ellipsoidal particle in a shear flow. *J. Fluid Mech.* 120:27–47, 1982.
- <sup>14</sup>Olla, P. Simplified model for red cell dynamics in small blood vessels. *Phys. Rev. Lett.* 82:453–456, 1999.
- <sup>15</sup>Pozrikidis, C. Numerical simulation of the flow-induced deformation of red blood cells. *Ann. Biomed. Eng.* 31:1194–1205, 2003.
- <sup>16</sup>Pries, A. R., K. Ley, M. Claassen, and P. Gaehtgens. Red cell distribution at microvascular bifurcations. *Microvasc. Res.* 38:81–101, 1989.
- <sup>17</sup>Secomb, T. W. Flow-dependent rheological properties of blood in capillaries. *Microvasc. Res.* 34:46–58, 1987.
- <sup>18</sup>Secomb, T. W. Mechanics of blood flow in the microcirculation. *Symp. Soc. Exp. Biol.* 49:305–321, 1995.
- <sup>19</sup>Secomb, T. W. Mechanics of red blood cells and blood flow in narrow tubes. In: *Hydrodynamics of Capsules and Cells*, edited by C. Pozrikidis. Boca Raton, Florida: Chapman & Hall/CRC, 2003, pp. 163–196.
- <sup>20</sup>Secomb, T. W., and R. Hsu. Non-axisymmetrical motion of rigid closely fitting particles in fluid-filled tubes. *J. Fluid Mech.* 257:403–420, 1993.
- <sup>21</sup>Secomb, T. W., and R. Hsu. Motion of red blood cells in capillaries with variable cross-sections. *J. Biomech. Eng.* 118:538–544, 1996.
- <sup>22</sup>Secomb, T. W., and R. Skalak. A two-dimensional model for capillary flow of an asymmetric cell. *Microvasc. Res.* 24:194–203, 1982.
- <sup>23</sup>Secomb, T. W., R. Skalak, N. Ozkaya, and J. F. Gross. Flow of axisymmetric red blood cells in narrow capillaries. *J. Fluid Mech.* 163:405–423, 1986.
- <sup>24</sup>Sugihara-Seki, M., T. W. Secomb, and R. Skalak. Two-dimensional analysis of two-file flow of red cells along capillaries. *Microvasc. Res.* 40:379–393, 1990.
- <sup>25</sup>Sun, C., and L. L. Munn. Particulate nature of blood determines macroscopic rheology: A 2-D lattice Boltzmann analysis. *Biophys. J.* 88:1635–1645, 2005.
- <sup>26</sup>Tran-Son-Tay, R., S. P. Sutera, and P. R. Rao. Determination of red blood cell membrane viscosity from rheoscopic observations of tank-treading motion. *Biophys. J.* 46:65–72, 1984.
- <sup>27</sup>Zhou, H., and C. Pozrikidis. The flow of ordered and random suspensions of two-dimensional drops in a channel. *J. Fluid Mech.* 255:103–127, 1993.